



## Studies on preparation and characterization of SiO<sub>2</sub>-CaO-P<sub>2</sub>O<sub>5</sub> and SiO<sub>2</sub>-CaO-P<sub>2</sub>O<sub>5</sub>-Na<sub>2</sub>O bioglasses substituted with ZnO

S. Chajri<sup>1</sup>, S. Bouhazma<sup>1</sup>, S. Herradi<sup>1</sup>, H. Barkai<sup>2</sup>, S. Elabed<sup>2</sup>, S. Ibsouda Koraichi<sup>2</sup>,  
B. El Bali<sup>1</sup> and M. Lachkar<sup>1\*</sup>

<sup>1</sup>Engineering Laboratory of Organometallic and Molecular Materials (CNRST, URAC 19), Faculty of Sciences, University Sidi Mohamed Ben Abdellah, Po. Box 1796 (Atlas), 30000 Fez, Morocco.

<sup>2</sup>Laboratory of Microbial Biotechnology, Faculty of Sciences and Technology, University Sidi Mohamed Ben Abdellah, 30000 Fez, Morocco.

Received 31 Jan 2015, Revised 17 Sep 2015, Accepted 18 Sep 2015

\*Corresponding Author. E-mail: [lachkar.mohammed@gmail.com](mailto:lachkar.mohammed@gmail.com); Tel: (+212671556742)

### Abstract

Bioglasses are important bioactive materials as they are used for the repair and reconstruction of bone tissues, by exhibiting direct bonding with them. We used a sol-gel method to produce the bioglass powders in the systems SiO<sub>2</sub>-CaO-Na<sub>2</sub>O-P<sub>2</sub>O<sub>5</sub>, SiO<sub>2</sub>-CaO-P<sub>2</sub>O<sub>5</sub>-ZnO and SiO<sub>2</sub>-CaO-Na<sub>2</sub>O-P<sub>2</sub>O<sub>5</sub>-ZnO. These glasses featured SiO<sub>2</sub> contents in the range 40-65 mol %, 22-24 mol% of CaO, 2-6 mol % of P<sub>2</sub>O<sub>5</sub>, 20.5-24 mol % of Na<sub>2</sub>O and 4.5-15.5 mol% of ZnO. The formed crystalline phases were identified using X-ray diffraction. Infrared spectra of the bioglasses were measured before and after immersion in simulated body fluid and the results were compared with the same behavior for the parent bioglasses. Experimental results indicate the formation of two main crystalline phases of sodium calcium silicate (Na<sub>2</sub>CaSi<sub>3</sub>O<sub>8</sub>, Na<sub>2</sub>CaSi<sub>3</sub>O<sub>9</sub>) according to the change in the bioglass composition. The effect of introduction of ZnO in SiO<sub>2</sub>-CaO-Na<sub>2</sub>O-P<sub>2</sub>O<sub>5</sub> system leads to the formation of a new crystalline phase of hexasodium tricalcium cyclohexasilicate (Na<sub>6</sub>Ca<sub>3</sub>Si<sub>6</sub>O<sub>18</sub>). The *in vitro* studies showed the formation of an apatite-like layer covering areas of the material surface. The influence of both chemical and morphological factors on the *in vitro* bioactivity has been studied. The apparent density and contact angle variation with time were measured.

**Keywords:** Bioactive glasses, Sol-gel, Zinc, *in vitro* bioactivity, Hydroxyapatite, Contact angle.

### Introduction

Bioactive glasses are a group of bioactive ceramic materials. A bioglass composition is commonly based on SiO<sub>2</sub> and P<sub>2</sub>O<sub>5</sub> for glassy network formers, and on CaO and Na<sub>2</sub>O for network modifiers; only some of the possible compositions are bioactive [1]. Bioglasses are surface reactive biomaterials used as implant materials in the human body to repair and replace diseased or damaged bone. The first kind of bioactive glass, called Bioglass® 45S5 was synthesized by Hench and coworkers [1]. The Bioglass® is composed of (wt%) 45SiO<sub>2</sub>, 24.5CaO, 24.5Na<sub>2</sub>O and 6P<sub>2</sub>O<sub>5</sub> [2]. Due to its good bioactivity, osteoconductivity and osteostimulative properties, this bioglass has been used in applications such as bone graft or filler [3], dental [4], cranio-maxillofacial applications [5] and implant coatings [6]. Bone-bonding ability also known as 'bioactivity' of a biomedical material is characterized by the formation of apatite layer on the surface of the material when immersed in simulated body fluid (SBF), which simulates perfectly human plasma in terms of pH and ionic composition [7]. This apatite layer provides the bonding interface with the surrounding living tissue. The extent of apatite formation is known to correlate to the ability of the material to be compatible with the newly formed bone tissue *in vivo* [8]. Apatite layer formation was evident when bioactive glass come into contact with rat muscle in the *in vivo* test performed by Lusvardi *et al.* [9]. Thus, *in vitro* SBF test is often regarded as a preliminary test to investigate the bioactivity of a potential biomedical material. 45S5 Bioglass® remains at the fore, capable of bonding to both soft and hard tissues [10]. The mechanism of bonding to living tissue involves a sequence of reaction steps [11]. The first 5 steps are reactions occurring on the glass surface that entail rapid ion exchange of Na<sup>+</sup> with H<sup>+</sup> and H<sub>3</sub>O<sup>+</sup> followed by dissolution of the glass network, polycondensation reaction of surface silanols (Si-OH) to high surface area silica (SiO<sub>2</sub>) gel. In the second phase, the growing hydroxycarbonated apatite layer (HCA) on the surface of the glass acts as an ideal environment for the

subsequent 6 cellular reaction steps during which osteoblasts (stem cells) differentiate to form new bone and bond to the implant surface [11].

The application of bioactive glasses as load-bearing implants is limited due to their poor mechanical integrity. In this regard, inclusion of sodium in the glass network during the preparation and subsequent thermal treatment has a major advantage of enhancing its mechanical properties through the formation of  $\text{Na}_2\text{Ca}_2\text{Si}_3\text{O}_9$  crystalline phase [12]. This approach however often leads to chemically heterogeneous materials with incipient crystallization and some degree of possible contamination from chemicals used during the cooling or grinding procedures [13]. Also, inclusion of  $\text{Na}_2\text{O}$  increases solubility advantages of the materials in aqueous media, thereby facilitating host tissue-material interaction [14]. One of the concerns associated with crystallization is the possibility of affecting the biodegradability of the scaffold, an essential feature of tissue engineering scaffolds [15]. However, crystalline  $\text{Na}_2\text{Ca}_2\text{Si}_3\text{O}_9$  formed in 45S5 Bioglass® during sintering transforms to a degradable amorphous calcium phosphate when the scaffold is incubated in an aqueous solution similar to biological fluids [15]. Another important advantage is that inclusion of Na, coupled with the high specific surface area of sol-gel-derived bioactive glasses, could lead to higher dissolution rates of the final materials in aqueous media as an important factor for the interaction of the material with living tissues [14].

Few methods have been developed to prepare the bioglasses. Melting method remains the traditional one generally used [16], since it is simple and suitable for massive production. However, during the high temperature stage, the volatile component  $\text{P}_2\text{O}_5$  tends to escape. In the early 1990s, sol-gel methods were introduced for bioglasses synthesis. They present relevant advantages compared to standard melt-quenching techniques [17]. In fact, the reaction taking place at low temperatures avoid the loss of  $\text{P}_2\text{O}_5$  by evaporation [18]. Moreover, the range of glass composition that is bioactive increases eg. up to 90 mol% silica based sol-gel derived bioactive glasses are bioactive compared to the upper limit of 60 mol% silica of melt-derived bioactive glass [19]. Bioactive glasses of various compositions synthesized by sol-gel method have shown minimal inflammatory response [20] and promote bone regeneration [21]. In particular, these methods extended the  $\text{SiO}_2$  limit to about 90 mol% beyond which the samples lose their bioactivity [19]. The bioactivity of glass can also be improved by adding intermediate or modifying oxides to the base compositions. Indeed, the addition of  $\text{ZnO}$  to standard bioglass could stimulate osteoblast proliferation and differentiation, thus improving the implant's ability to bond with bone [22]. Zinc, as the most abundant trace metal in bone mineral, is an essential element that has stimulatory effects on bone formation *in vitro* and *in vivo* as well as inhibitory effects on osteoclastic bone resorption *in vivo* [23]. It can also promote bone metabolism and growth, increase bone density and prevent bone loss [24]. In fact, the slow release of zinc incorporated into an implanted material promotes bone formation around the implant and accelerates the patient's recovery [25]. In particular, zinc promotes the bioglass chemical durability in aqueous solutions such as body fluids, and improves its mechanical properties [25]. Recently, it was shown that zinc extends the specific surface area and thereby the number of sites for the nucleation of calcium phosphate precipitates in binary  $\text{SiO}_2$ -CaO sol-gel glasses [26]. Zinc is necessary in the function of all cells, binding specific DNA regions to regulate genetic control of cell proliferation [27]. It is also reported to play a role in bone healing and metabolism [28], with anti-inflammatory roles [29]. It has been demonstrated that zinc (a) stimulates bone formation *in vitro* by activating protein synthesis in osteoblast cells, (b) increases ATPase activity in bone [28] and inhibits bone resorption of osteoclast cells in mouse marrow cultures [28], and (c) has regulatory effects on bone cells and, thus, on gene expression [30]. Nonetheless, it has been well documented that an excess of zinc may cause anemia or reduced bone formation [27] as well as systemic cytotoxicity. In addition, zinc has a number of positive effects on the body, for example; the ability to increase the deoxyribonucleic acid (DNA) of osteoblasts [31], resulting in increased bone mass [32], and antibacterial effects [33].

We focus in this paper the study of the influence of Zn, as a doping element, on the bioactivity of the ternary  $\text{SiO}_2$ -CaO- $\text{P}_2\text{O}_5$  and the quaternary  $\text{SiO}_2$ - $\text{Na}_2\text{O}$ -CaO- $\text{P}_2\text{O}_5$  glasses. For this purpose, Zn doped  $\text{SiO}_2$ -CaO- $\text{P}_2\text{O}_5$  and  $\text{SiO}_2$ - $\text{Na}_2\text{O}$ -CaO- $\text{P}_2\text{O}_5$  bioactive glasses were elaborated using a sol-gel method and tested by immersion in biological fluids for different periods. The bioactivity after immersion in Simulated Body Fluid (SBF) was investigated. The evolution of the biological fluids composition was followed by ICP-AES (Inductively Coupled Plasma-Atomic Emission Spectroscopy) analyses. The physicochemical properties of the prepared powder samples were characterized using several methods such as X-ray diffraction (XRD), Fourier transform infrared spectroscopy (FTIR) and Environmental Scanning Electron Microscopy (ESEM). The surface wettability of samples was estimated by contact angle measurements and their apparent densities were measured.

## 2. Materials and methods

### 2.1. Materials

The following chemicals were used as precursors for the synthesis of the sol-gel 46qA, 65qn, 64qn, 60qn, 45pnA, 44pnA and 40pnA materials (see Table 1): tetraethyl orthosilicate (TEOS) (Sigma-Aldrich, 99%), triethyl phosphate (TEP) (Merck Schuchardt, 99%), sodium nitrate (PANREAC, 99%), calcium nitrate tetrahydrate (Loba Chemie, 98%), zinc nitrate (Sd Fine Chem Limited, 98%), nitric acid (Prolabo, 65%-69%) and deionized water.

### 2.2. Preparation of the bioglasses

Figure 1 illustrates schematically the process followed to obtain the bioglasses in  $\text{SiO}_2\text{-CaO-Na}_2\text{O-P}_2\text{O}_5$ ,  $\text{SiO}_2\text{-CaO-P}_2\text{O}_5\text{-ZnO}$  and  $\text{SiO}_2\text{-CaO-Na}_2\text{O-P}_2\text{O}_5\text{-ZnO}$  systems. Compositions of the bioglasses used for *in vitro* tests are summarized in Table 1. A bioglass is prepared by hydrolysis and polycondensation of tetraethyl orthosilicate (TEOS), triethylphosphate (TEP),  $\text{NaNO}_3$ ,  $\text{Ca}(\text{NO}_3)_2 \cdot 4\text{H}_2\text{O}$  and  $\text{Zn}(\text{NO}_3)_2 \cdot 6\text{H}_2\text{O}$ . Nitric acid (2N  $\text{HNO}_3$ ) is used to catalyze the TEOS and TEP hydrolysis, using a molar ratio of  $(\text{HNO}_3 + \text{H}_2\text{O})/\text{TEOS} = 6$ . Each of the reactants was consecutively added in 1 hour intervals under continuous stirring. Next, the sol was cast in containers and kept at  $25^\circ\text{C}$  for 3 days to allow the hydrolysis and polycondensation reactions, up until the formation of a viscous gel. For aging, the gel was stored in the sealed container and kept at  $70^\circ\text{C}$  for 3 days. The drying of the gel was carried out at  $150^\circ\text{C}$  for 52 h. A dry gel in powder form was stabilized by heating in air at  $700^\circ\text{C}$  for 3h to obtain bioglass. Different compositions of bioglasses are listed in Table 1.

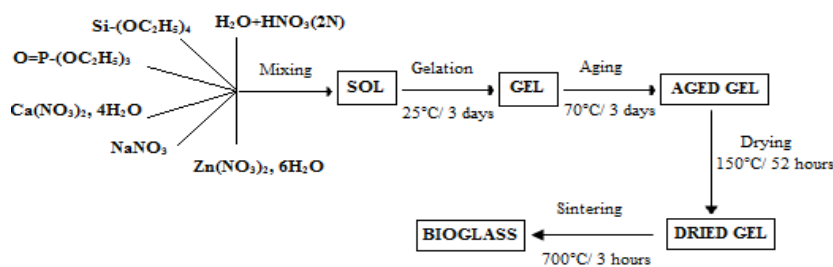


**Figure 1:** Schematic illustration of the process followed for preparation of bioglasses.

**Table 1:** Chemical composition of the bioglasses (mol %).

Sample	$\text{SiO}_2$	$\text{CaO}$	$\text{Na}_2\text{O}$	$\text{P}_2\text{O}_5$	$\text{ZnO}$
46qA	46	24	24	6	---
65qn	65	24	---	6	5
64qn	64	23	---	5.5	7.5
60qn	60	22	---	2.5	15.5
45pnA	45	23	22	5.5	4.5
44pnA	44	22	21.5	5	7.5
40pnA	40	22.5	20.5	2	15

### 2.3. Characterizations

#### 2.3.1. X-ray diffraction

X-Rays investigations from the bioglasses samples were carried out with X'Pert Pro X-ray diffractometer, using a  $\text{Cu\_K}\alpha$ -radiation ( $\lambda=1.5418 \text{ \AA}$ ). The equipment was calibrated using an external standard. The X-ray diffraction patterns were recorded in a  $2\theta$ -range [ $10\text{-}60^\circ$ ]. The results were analyzed and compared with data of the database.

#### 2.3.2. Infrared spectroscopy

Infrared absorption spectra of the samples were measured at room temperature in the wave number range of  $4000\text{-}400 \text{ cm}^{-1}$  using a Fourier transform infrared spectrometer (VERTEX 70 FT-IR).

### 2.4. In vitro bioactivity tests

In 1991, Kokubo proposed the concept of *in vitro* bioactivity test which is carried out in simulated body fluid instead of living body [8]. Then after, the test became the most widely used solution for *in vitro* investigation of

bioactivity of bioactive materials. The ion concentration of simulated body fluid (SBF) is nearly equal to that of human blood plasma and is given in Table 3 [8]. The simulated body fluid solution was prepared as described by Kokubo [34] by dissolving the required amounts of reagent grade chemicals (Table 2), sodium chloride (NaCl), sodium bicarbonate (NaHCO<sub>3</sub>), potassium chloride (KCl), dipotassium hydrogen phosphate (K<sub>2</sub>HPO<sub>4</sub>·3H<sub>2</sub>O), magnesium chloride hexahydrate (MgCl<sub>2</sub>·6H<sub>2</sub>O), calcium chloride dihydrate (CaCl<sub>2</sub>·2H<sub>2</sub>O) and sodium sulphate (Na<sub>2</sub>SO<sub>4</sub>) in deionized water. It was buffered at a pH value of 7.4 with 50 mM tris(hydroxymethyl)aminomethane (NH<sub>2</sub>C(CH<sub>2</sub>OH)<sub>3</sub>) and 1N hydrochloric (HCl) acid at the temperature 37 °C. We carried out *in vitro* studies by soaking 90 mg bioactive glass sample in 45 ml SBF solution, at the temperature 37 °C, for 7, 14 and 21 days. After soaking, the samples were filtered, rinsed with acetone, and dried in a desiccator before any characterization. All the reacted SBF solution was saved for Inductively Coupled Plasma analysis to measure ionic concentration of Si, Ca, Na, P and Zn in SBF solution. In addition, the SBF solution was also monitored for changes in pH before and after.

**Table 2:** Reagents for preparing the SBF solution.

Order	Reagent	Amount
1	NaCl	7.996 g
2	NaHCO <sub>3</sub>	0.350 g
3	KCl	0.224 g
4	K <sub>2</sub> HPO <sub>4</sub> ·3H <sub>2</sub> O	0.228 g
5	MgCl <sub>2</sub> ·6H <sub>2</sub> O	0.305 g
6	1M-HCl	40 mL
(About 90 % of total amount of HCl to be added)		
7	CaCl <sub>2</sub>	0.278 g
8	Na <sub>2</sub> SO <sub>4</sub>	0.071 g
9	(CH <sub>2</sub> OH) <sub>3</sub> CNH <sub>2</sub>	6.057 g

**Table 3:** Ion concentrations (mM) of SBF and human blood plasma.

Ion	Simulate Body Fluid	Blood plasma
Na <sup>+</sup>	142.0	142.0
K <sup>+</sup>	5.0	5.0
Mg <sup>2+</sup>	1.5	1.5
Ca <sup>2+</sup>	2.5	2.5
Cl <sup>-</sup>	148.8	103.0
HCO <sub>3</sub> <sup>-</sup>	4.2	27.0
HPO <sub>4</sub> <sup>2-</sup>	1.0	1.0
SO <sub>4</sub> <sup>2-</sup>	0.5	0.5

### 2.5. Apparent porosity measurements

Arthur method was employed to obtain the porosity (P<sub>0</sub>) of bioactive glass using distilled water and xylen. Porosity (P<sub>0</sub>) of samples was obtained employing the relation (1) as given below:

$$(1) \quad P_0 = \frac{(m_2 - m_1)}{(m_2 - m_3)} \times \frac{\rho_{\text{water}}}{\rho_{\text{xylen}}}$$

where m<sub>1</sub> is the weight of sample in air, m<sub>2</sub> and m<sub>3</sub> are the weights after soaking respectively in xylen and water, ϕ<sub>water</sub> is the density of water and ϕ<sub>xylen</sub> is the density of xylen.

### 2.6. Contact angle measurements

Contact angle measurements were performed on 46qA, 45pnA, 44pnA, 40pnA, 65qn, 64qn and 60qn surfaces for studying the degree of hydrophilicity of their surfaces. Used liquids were distilled water and simulated body fluid solution. The wettability was determined by the sessile-drop contact angle method with a contact-angle goniometer by the sessile drop method (GBX-France) [35]. A drop (~ 1μL) of water is placed on the glass disk, fixed on a prepared plate of substratum, and the image is immediately sent *via* the camera to the computer for analysis. Water contact angles were measured after a delay of 5s to ensure the equilibration of the droplet

(Figure 2). The measurements were repeated by depositing at least three drops on each substrate, and final results were presented by the average of measured drops. On the other hand, the bioactive glass disks were prepared using a compression molding method. The bioactive glass powders were compression molded in a stainless steel mould into compact disks with the dimension of 13 mm in diameter and 2 mm in thickness. The compression molding press was operated at a pressure of 10 MPa.

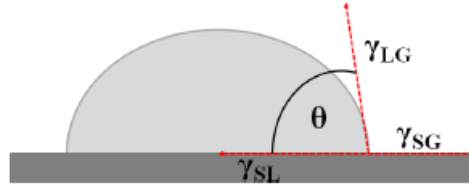


**Figure 2:** The droplet is formed on three different interfaces between the droplet, substrate and air resulting in equilibrium of their interfacial energies;  $\gamma_{LG}$  liquid/vapor,  $\gamma_{SL}$  solid/liquid and  $\gamma_{SG}$  solid/air. The angle  $\theta$  was determined after the drop reached the equilibrium state.

### 2.7. Environmental Scanning Electron Microscopy analysis

Morphological characterization of the pellets, regarding the surface modifications that occurred during the *in vitro* bioactivity test, was performed by Environmental Scanning Electron Microscopy. A set of samples was selected and analyzed before and after soaking in SBF solution at different testing times.

## 3. Results and discussion

### 3.1. XRD analysis of bioglass

Generally, bioactive glass with heat treatment around 973 K is expected to be amorphous as the crystallization is known to occur at temperature around 1073 K [36] and even above [37]. The X-ray diffraction patterns of Na-free and Zn-doped bioactive glass samples (60qn), (64qn) and (65qn) did not show any diffraction picks, see Figure 3, which confirms their amorphous natures.

In contrary, crystallization seems to occur in the samples (46qA), (40pnA), (44pnA) and (45pnA) (see Figure 4). In fact pattern of bioactive glass sample (46qA) shows the presence of two main crystalline phases of sodium calcium silicate, namely  $\text{Na}_2\text{Ca}_2\text{Si}_3\text{O}_9$  and  $\text{Na}_2\text{CaSi}_3\text{O}_8$ . Our results are in agreement with previous related publications [1, 38]. The effect of introduction of ZnO in place of  $\text{SiO}_2$ , to the bioactive glass (46qA) is shown to lead to the formation of a new crystalline phase of hexasodium tricalcium cyclohexasilicate of the formula ( $\text{Na}_6\text{Ca}_3\text{Si}_6\text{O}_{18}$ ). Furthermore, it is envisioned that inclusion of  $\text{Na}_2\text{O}$  in the glass network will facilitate crystallization of certain sodium calcium silicate phases, such as  $\text{Na}_2\text{Ca}_2\text{Si}_3\text{O}_9$  which ultimately will improve their mechanical properties [39].

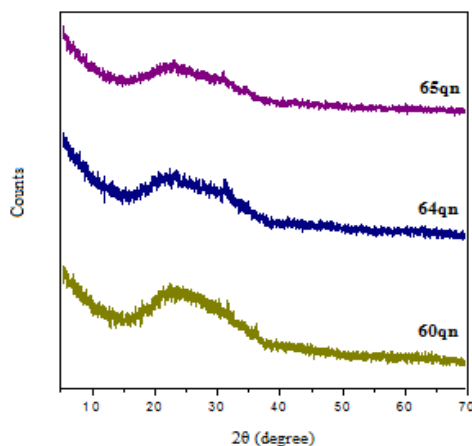


**Figure 3:** XRD patterns of 60qn, 64qn and 65qn.

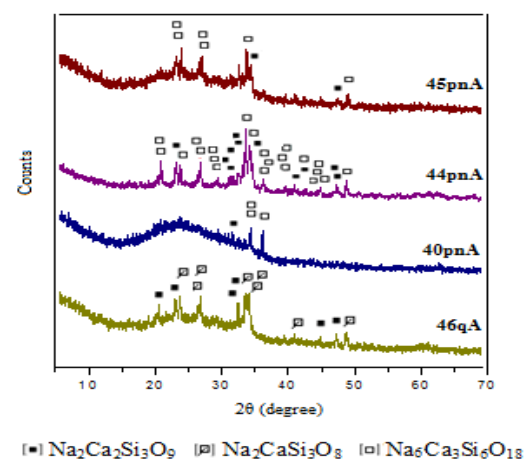


**Figure 4:** XRD patterns of 46qA, 40pnA, 44pnA and 45pnA.

### 3.2. Bioactivity analysis

The bioactivity of a material to form bone-like apatite can reflect its potential for bonding with the bone [40]. The bioactive character of our samples was tested *in vitro* by analyzing the apatite formation at the material surface after soaking in SBF. The nature of the apatite layer formed was further characterized by XRD (Fig. 5).

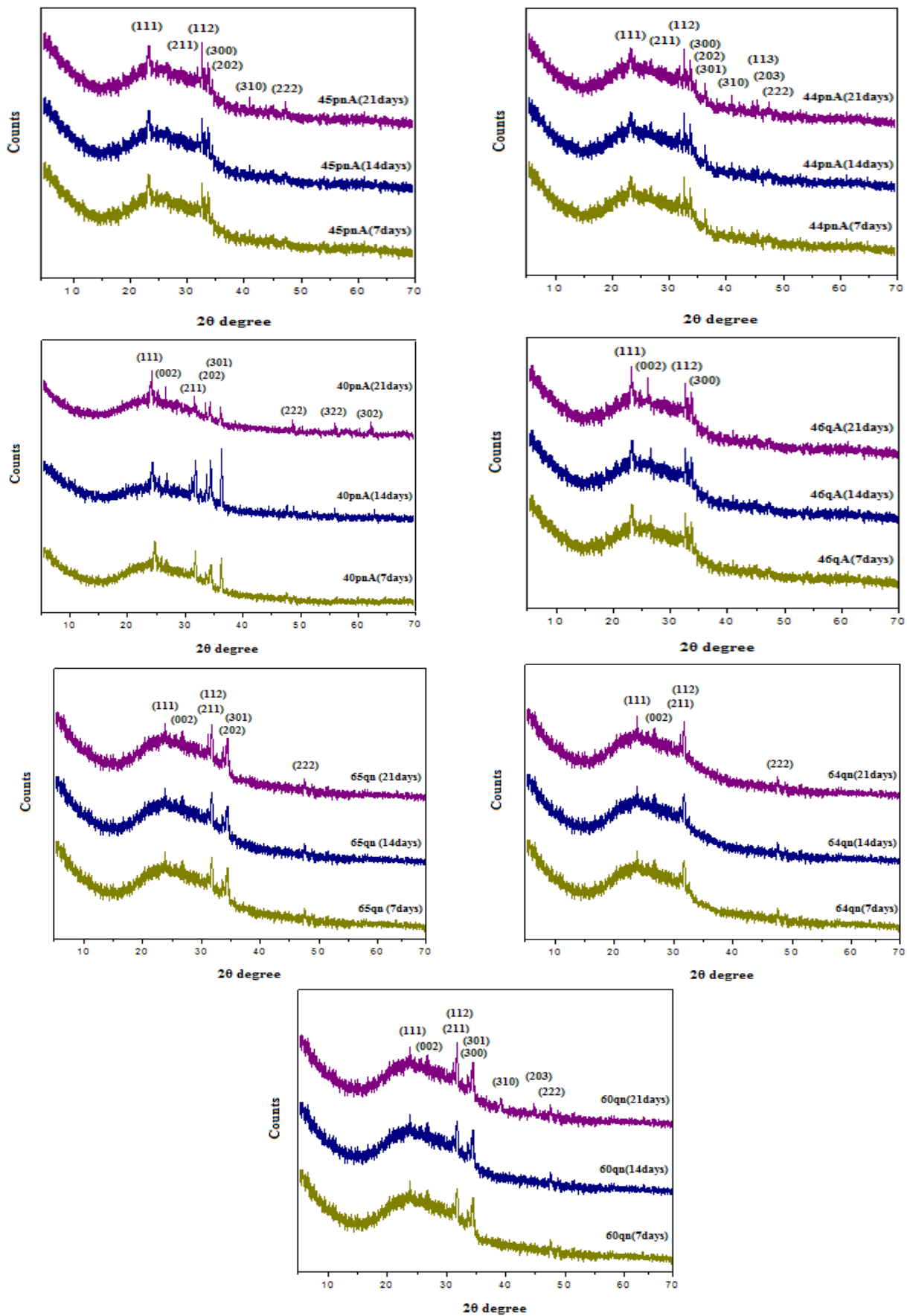


**Figure 5:** XRD patterns of bioactive glasses 46qA, 45pnA, 44pnA, 40pnA, 65qn, 64qn and 60qn before and after soaking for 7, 14 and 21 days in SBF solution.

The XRD patterns of 46qA, 45pnA, 44pnA, 40pnA, 65qn, 46qn and 60qn, after immersion in SBF, showed some differences in their crystallization. A Ca-P layer forms on the surface of all samples upon 7 days of immersion. After which, the significant reflection peaks of HAp (111), (211), (112), (202), (300), (301) and (222) are observed. The intensities of these reflections increase with the duration of immersion [41]. With a long exhibition, other apatite's peaks appear, these are assigned to the reflections (002), (202) and (203), (302), (322), (113) and (310) from the HAp. These results ensured the deposition of HAp on all glass samples.

All synthesized bioglasses have been shown to be bioactive because of their ability to produce biologically compatible apatite. These bioglasses release some of their components in phosphate-containing fluid, triggering the initial precipitation of amorphous calcium phosphates, which act as precursors for the formation of apatite. This spontaneous precipitation promotes a biomineralization process that leads to the formation of an interfacial layer with tag-like-structures at the biomaterial interface. The ability to induce the formation of apatite allows the integration of the biomaterial into the environment [42].

### 3.2. FTIR spectra of bioglasses

Infrared spectra of the bioglasses were measured before and after treatment with SBF solution, for 7 to 21 days. The spectra were correlated, before and after immersion in SBF, and were compared with literature [43, 44]. The assignments of functional groups to different bands in the spectra of the title compounds, compared to literature, are shown in Table 4. The degree of bioactivity in bioglasses is usually expressed by the formation of hydroxyl-carbonate apatite surface layer which is followed by the process of its crystallization [10]. The stages or sequences of the formation of hydroxyapatite as suggested by Hench [10] can be correlated with the changes or differences in the infrared reflection spectra after prolonged immersion of the bioglass in SBF as seen in Table 5. The IR spectra of all bioactive glasses before immersion in SBF solution reveal Si-O-Si bending ( $500-400\text{ cm}^{-1}$ ), Si-O stretching ( $940-860\text{ cm}^{-1}$ ) and Si-O-Si stretching (asymmetric) ( $1200-970\text{ cm}^{-1}$ ) bands, which are known and accepted to be mainly characteristic of silicate network [45]. This may be attributed to the presence of major  $\text{SiO}_2$  as a basic building constituent. The IR spectra of (46qA), (45pnA), (44pnA) and (40pnA) show the additional bands at wavenumbers  $570-580\text{ cm}^{-1}$  which are due to the presence of sodium calcium silicate crystalline phase [46]. The spectra of Na free and Zn doped bioactive glass samples (60qn), (64qn) and (65qn) show disappearance of the IR band around  $580-570\text{ cm}^{-1}$ , which confirms their amorphous nature. Those of (46qA), (45pnA), (44pnA), (40pnA), (60qn), (64qn) and (65qn), after soaking in SBF solution for different times, reveal Si-O-Si stretching (symmetric) ( $720-840\text{ cm}^{-1}$ ) and (asymmetric) ( $1000-1100\text{ cm}^{-1}$ ) bands, which indicates the formation of silica-rich layer. The presence of P-O bending (amorphous) ( $560-600\text{ cm}^{-1}$ ) bands indicates the formation of  $\text{CaO-P}_2\text{O}_5$  layer. Emerging of P-O bending (crystalline) ( $500-560\text{ cm}^{-1}$ ) bands reveals the formation of hydroxycarbonated apatite (HCA) layer. Presence of O-H stretching ( $2600-3800\text{ cm}^{-1}$ ), C-O stretching ( $800-890\text{ cm}^{-1}$ ) and ( $1400-1530\text{ cm}^{-1}$ ) bands shows the crystalline nature of HCA layer and P-O stretching ( $910-1040\text{ cm}^{-1}$ ) bands are attributed to presence of HCA layer [12, 44]. The hydroxycarbonated apatite layer formed on the surface of the bioglass and the slight change in the peaks intensity as the soaking time increases, have been already reported in the literature [1, 12]. Table 5 gives correlation between spectral frequencies and functional groups in a bioactive glass and steps of bioactivity [47]. In addition, the spectra of all bioactive glasses reveal Si-O-Si bands at  $400-500\text{ cm}^{-1}$  (bending vibration),  $720-840\text{ cm}^{-1}$  (bending vibration) and  $1000-1100\text{ cm}^{-1}$  (stretch vibration). These confirm the presence of a silica gel [48]. The apparition of apatite mineral and a silica gel highlight the interactions between the biomaterials and the physiological solution as described by Hench *et al.* [1]. This mechanism could be explained through the following steps: (a) rapid exchange of protons  $\text{H}_3\text{O}^+$  from the physiological solution with  $\text{Ca}^{2+}$  and  $\text{Na}^+$  ions in bioglass to form the Si-OH groups, (b) loss of soluble silica as  $\text{Si}(\text{OH})_4$  by breaking of Si-O-Si bridging links and subsequent formation of surface silanol groups in the process, (c) condensation and repolymerization of surface silanols to form  $\text{SiO}_2$ -rich surface layer, (d) migration of  $\text{Ca}^{2+}$  and  $\text{PO}_4^{3-}$  ions through the surface silica-rich layer and formation of a Ca-P rich layer on the surface of the bioglass, (e) incorporation of  $\text{OH}^-$  and  $\text{CO}_3^{2-}$  ions from the solution and subsequent crystallization of the Ca-P layer to form HCA [1]. The obtained results confirm the bioactivity of all synthesized samples.

Careful inspection of FTIR transmittance spectra of all the ZnO substituted bioactive glasses (i.e.: 45pnA, 44pnA, 40pnA, 65qn, 64qn and 40qn) in comparison with the base bioactive glass (46qA) reveals minor or limited variation of the positions and intensities of the transmittance peaks. The main differences can be summarized in bioactive glasses, where there was a time delay in the formation of peaks. After soaking in SBF solution it was observed that the intensity of peak decreased with increasing ZnO content. The FTIR

transmittance spectra of bioactive glasses after soaking in a SBF solution indicates that as well as ZnO content increases a decrease in the formation of HCA layer was observed. This can be due to the fact that the release of Si from the bioactive glass decreases with increasing of ZnO content in it since ZnO enhances the chemical stability of silicate glasses [49]. FTIR transmittance spectra showed that the introduction of zinc in the vitreous matrix has the effect of greatly modifying the kinetics of formation and crystallization of the hydroxyapatite layer. This result is in agreement with the results published by Mosbahi et al [50]. Therefore, the suppression of the formation of silica-rich layer leads to the suppression of CaO-P<sub>2</sub>O<sub>5</sub> layer, and hence suppression of the formation of HCA surface. The IR spectra of crystalline phases (46qA, 45pnA, 44pnA and 40pnA) and amorphous phases (65qn, 64qn and 60qn) after soaking in SBF solution show that the formation of HCA layer on crystalline phases are significantly less than the amorphous phase. This phenomenon might be explained by considering that the amorphous phase is usually more prone to ion leaching phenomena than crystalline phases [51].

**Table 4:** Correlation between wavenumber at which transmittance bands emitted and functional groups in bioactive glasses after immersing in SBF.

Wavenumber (cm <sup>-1</sup> )								Published data [43, 44]	Vibration mode
This work									
Period (d)	46qA	45pnA	44pnA	40pnA	65qn	64qn	60qn		
7	1415	1415	1414	1411				1530-1400	C–O stretching
14	1421	1465	1450	1412					
21	1418	1475	1407	1387					
7								1200-1100	P–O stretching
14									
21									
7	1016	1021	1009	1002	1033	1050	1036	1100-1000	Si–O–Si stretching
14	1012	1016	1011	1002	1026	1048	1036		
21	1018	1018	1012	1008	1043	1034	1028		
7								1045, 1025	P–O stretching
14									
21									
7				950				1040-910	P–O stretching
14		950	975						
21		975	950	950					
7			875					940-860	Si–O–Si stretching of non-bridging oxygen atoms
14									
21	874			850					
7								890-800	C–O stretching
14	878								
21									
7					796	801		840-720	Si–O–Si symmetric stretch of bridging oxygen atoms between tetrahedra
14					791	797			
21	784	850	825	837	788	798, 806			
7		576	585	565	566			600-560	P–O bending (amorphous)
14		561	585	562					
21	578	565	566.80			595.5, 600			
7	554							560-500	P–O bending (crystal)
14	565				554.05	548.85			
21	558			537.5	551.05		525, 550		
7	435	417	450	420	439	417, 445	420, 433, 460	500-400	Si–O–Si bending
14	446	416	420	415	448	415, 448, 460	409, 458		
21	449	441	413, 451	410	439, 458	450	450, 420		

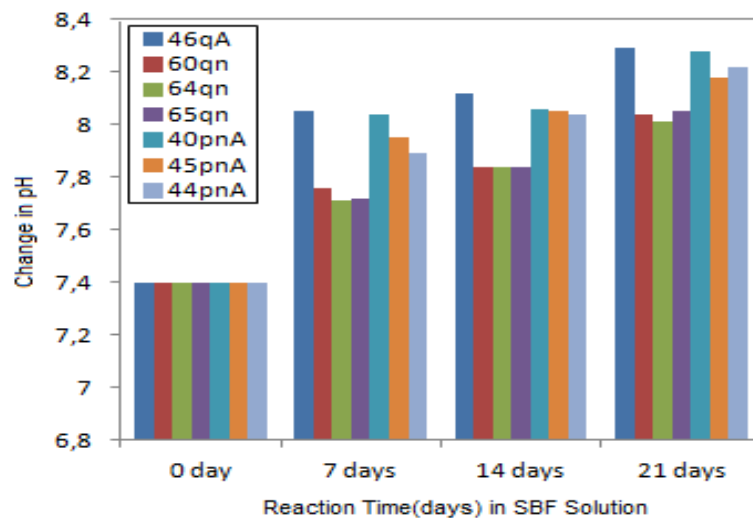
### 3.3. Chemical durability of bioglass (changes in pH)

Figure 6 shows the pH change vs. time for all the bioglasses. These results, show that for all samples the pH varies with compositions for given periods, within 7 to 21 days. They are compared to the initial pH of the

solution (pH = 7.4) which is due to the fast release of Na<sup>+</sup> and Ca<sup>2+</sup> ions through exchange with H<sub>3</sub>O<sup>+</sup> ions into the solution [52]. The changes in pH are due to ion leaching i.e. chemical changes of material surfaces at different time periods. The pH value of SBF solution increased during first 7 days of soaking. The reduction in the concentration of H<sup>+</sup> ion is due to the replacement of cation ions in the glass and subsequent production of OH<sup>-</sup> ions. It was also observed that the addition of ZnO in the base bioactive glass (46qA) as in Na free bioactive glass causes an initial decrease in the pH. For example, the pH value of 44pnA was lower than that for 40pnA during SBF immersion (Figure 6). This is probably due to the release of Zn ions into the SBF solution. Migration of Zn ions into the SBF solution causes it to become more acidic and explains the lower amount of pH for 44pnA during SBF immersion [18]. The Ca<sup>2+</sup> released into SBF and the increases in pH are in agreement with the mechanism proposed for HCA formation on the surfaces of bioactive glasses [53]. In such glasses, an interchange between the Ca<sup>2+</sup> ions of the glass and the H<sub>3</sub>O<sup>+</sup> of the solution takes place. This gives rise to the formation of Si-OH groups on the glass surface, inducing apatite nucleation [1]. The nucleation of HCA is possible because the surrounding fluid is supersaturated with respect to HCA due to the dissolution of the calcium ions. In addition, silica-rich interlayer dissolves a considerable amount of silicate ion and provides favorable sites for the nucleation. The process of nucleation and growth of the HCA layer continues by the reactions of the calcium, phosphate, and hydroxide ions. It is possible that carbonate or fluoride anions incorporate in the reactions, as well [54].

**Table 5:** Correlation between spectral frequencies and functional groups in bioactive glasses and the steps of surface changes after immersion in SBF [47].

Wavenumber (cm <sup>-1</sup> )	Vibrational mode	Surface reaction stages
860 - 940	Si-O (Stretch)	Stages 1 and 2
720 - 840	Si-O-Si (Tetrahedral)	Stage 3
560 - 600	P-O (Bend) (Amorphous)	Stage 4
500 - 560	P-O (Bend) (Crystalline)	Stage 5



**Figure 6:** pH of SBF solution that was taken before and after soaking of bioactive glasses for a period of 7, 14 and 21 days.

### 3.4. Changes in SBF composition

Figure 7 shows the profiles of dissolution of glass powders in SBF. It correlates the elemental concentrations of Si, Ca, P, Na and Zn, before and after different immersion's times for glass powders in SBF. For all samples, the concentration of silicon released into solution increases rapidly during the first 7 days of soaking and then it increases very strongly till the last day of immersion (14 days). The ranges of silicon concentration (ppm) in the SBF are as follow: (0-91.97) for 65qn, (0-98.76) for 64qn, (0-109.5) for 60qn, (0-99.31) for 45pnA, (0-97.49) for 44pnA and (0-112.4) for 40pnA. This concentration decreased then continuously till the last day of immersion (21 days). For 46qA, silicon ions concentration increased however during the time of immersion. The release of silicon ions indicates the first stage of dissolution by breaking up of the outer silica layers of the

network. The solid silica dissolves in the form of monosilicic acid  $\text{Si}(\text{OH})_4$  to the solution resulting from breakage of Si–O–Si bonds and formation of Si–OH (silanols) at the glass solution interface.

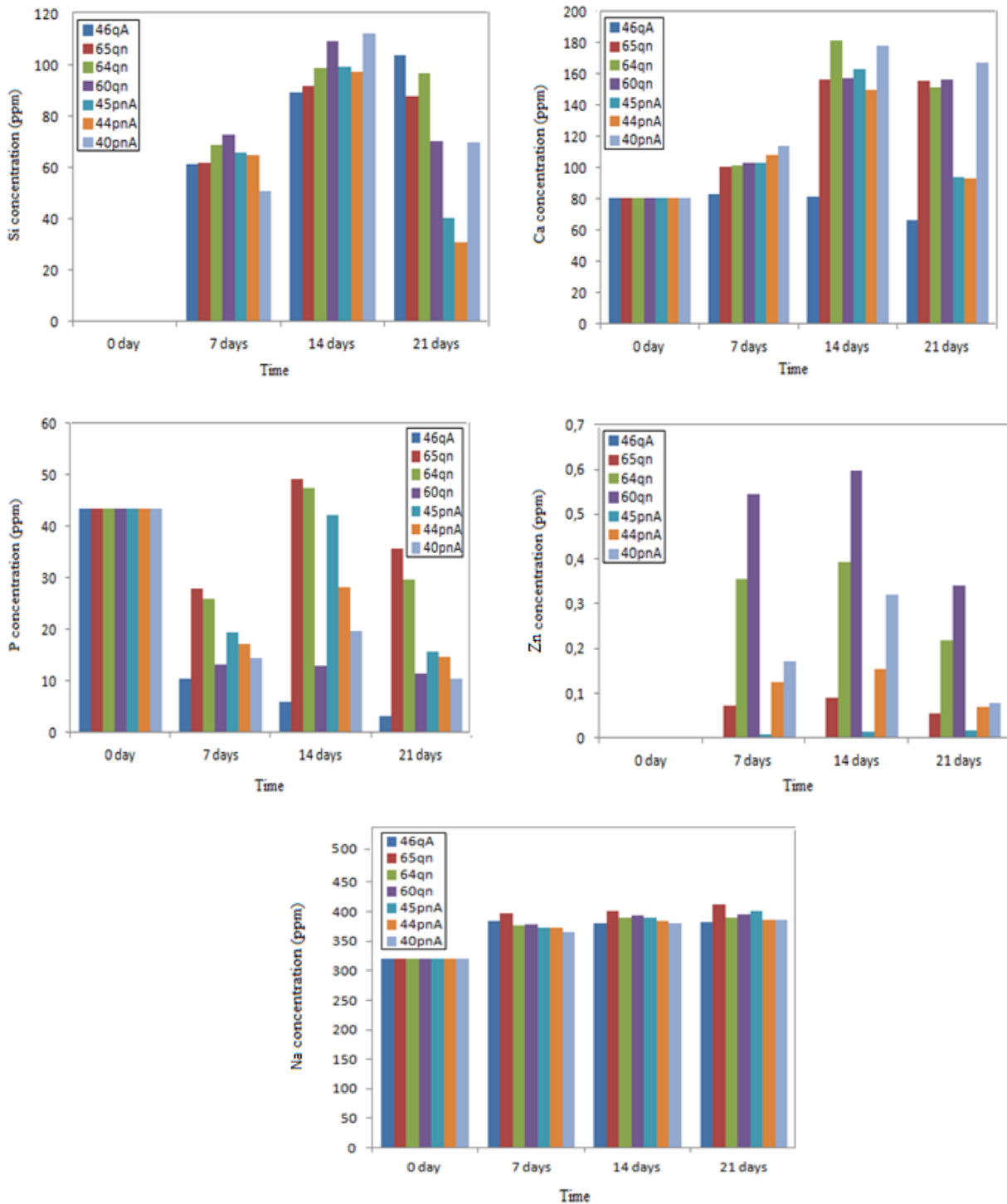


**Figure 7:** Si, Ca, P, Na and Zn concentrations in SBF solution that was taken before and after soaking of bioactive glasses for a period of 7, 14 and 21 days.

The concentrations of calcium and phosphorus ions in SBF solution versus soaking times are linked to the formation of HAp layer. Measurements of Ca and P concentrations allow evaluating the rate of biomineralization of biomaterials after immersion in physiological solution. Demineralization and

remineralization are natural processes which continuously occur for teeth. Physiological processes as well as bacterial acids and foods cause demineralization, while remineralization results from the deposition of mineral (calcium and phosphorous) from saliva or oral fluid. Since natural remineralization is not enough for having strong enamel, bioactive glasses are used to augment the process [55]. Bioactive glasses have unique remineralizing properties and are generally introduced into various dentifrices as very fine particles to provide calcium and phosphorus to the tooth surface [56]. Narayana et al confirmed that bioactive glass is an effective remineralizing agent as the effects of bioactive- containing products were investigated on remineralization of artificial induced carious enamel lesion [57]. In this study, the variations of calcium ions concentrations in SBF solution as a function of soaking time are shown in Figure 7. During the first 7 days of immersion, calcium ions concentration in the analyzed SBF solution increases gently for all bioactive glasses. This increase is coherent with the release of available calcium content from bioactive glass in the desalkalization process. For 65qn, 64qn, 60qn, 45pnA, 44pnA and 40pnA, the calcium ions concentration increases very strongly till the 14 days, and then after it decreases very strongly. This decrease corresponds to the precipitation of calcium ions on the surface of bioactive glass to form the apatite layer. For 46qA, calcium ions concentration decreased during the time of immersion. It was observed that the Na ions concentration increased rapidly during first 7 days of soaking and then it attains nearly a constant value where as Zn ions concentration increased during the first 7 day of soaking and then it decreased continuously (Figure 7). The slow release of zinc incorporated into the glass promotes bone formation around the implant and accelerates the patient's recovery [25]. Therefore, bioactive glass with slow release of Zn ions is an appropriate candidate for orthopedic applications [25]. It was also observed that the effect of introduction of ZnO in place of SiO<sub>2</sub>, to the bioactive glass (46qA) and to Na free bioactive glass decreases the leaching rate of ions. Figure 7 shows the variations of phosphorus ions concentrations in SBF as a function of soaking time. For (46qA), there is no increase of the phosphorus ions concentration after the first 7 days of immersion. This is probably due to the presence of Na that slows the dissolution of bioglass from the matrix of sample. The phosphorus ions concentration decreases also strongly since the beginning of the immersion. This could be attributed to consumption in the formation of hydroxyapatite layer on the surface. At 14 days of immersion, the (46qA) utilizes almost a large quantity of the phosphorus ions in the SBF solution to form the apatite layer, the phosphorus ions concentration is of 5 ppm and of 3 ppm after 21 days. This confirms the rapid formation of an apatite layer on the surface of (46qA) sample bioactive glass. For (65qn), (64qn), (60qn), (45pnA), (44pnA) and (40pnA), the phosphorus ions concentration increases after first 14 days of immersion. It corresponds to dissolution of a quantity of phosphorus from the matrix of bioactive glass. Furthermore, the phosphorus ions concentration decreases very fast till the last day of immersion because the phosphorus is used to form the layer of calcium phosphate on the surface of bioactive glass. After 21 days of immersion, the phosphorus's concentrations (ppm) are respectively 35.6 (65qn), 29.6 (64qn), 11.5 (60qn), 15.6 (45pnA), 14.7 (44pnA) and 10.42 (40pnA). According to these results, a large quantity of the phosphorus ions present in SBF is used to form the hydroxyapatite layer.

During initial period of soaking faster release of Ca ions increases the concentration of Ca ions. Decrease in Ca concentration is due to formation of CaO-P<sub>2</sub>O<sub>5</sub> layer. The decrease in P concentration with a simultaneous increase in Si concentration is consistent with the formation of CaO-P<sub>2</sub>O<sub>5</sub> layer. The participation of Zn in the nucleation process can be ascertained by the observed variation in its concentration with soaking time. The obtained results are in a good agreement with the analyses carried out by FTIR and XRD, which all confirm the bioactivity and biomineralization activity of all bioactive glasses samples.

### 3.5. Porosity measurements

Porosity of biomaterials is favored for facilitating the cell reorganizations and vascularization when applied inside physiological environment [58]. For a given bioactive glass scaffold, the porosity, pore size and pore inter-connectivity are critical parameters. In general, interconnected pores with a mean diameter (or width) between neighboring pores of 100 μm or greater, and open porosity of >50% are generally considered to be the minimum requirements to permit tissue ingrowth and function in porous scaffolds [59]. Trabecular bone, found at the end of long bones, in vertebrae and in flat bones such as the pelvis, is much more porous, with porosity in the range 50-90% [60]. Zinc has been known to encourage attachment, proliferation of osteoblast and increase alkaline phosphatase expression. The enzymes responsible for laying down the bone callus were activated by Zn, and Osteon and Osteoid structures are known to have a high Zn content. So zinc has an important role for the mineralization of bone [61]. Figures 8 and 9 show open porosity of all bioactive glasses with different ZnO concentrations. When increasing the ZnO doping concentration, the porosity of bioactive glasses samples

(40pnA), (44pnA), (45pnA), (60qn), (64qn) and (65qn) increased. This was possible that gel with high ZnO doping concentration had short aging time so that the gels became to higher viscosity and obtained many pores after gel casting or the sponge immersing. Previous studies demonstrated that the high porosity facilitated cells' proliferation, vascular in growth, and internal mineralized bone formation [62].

In addition, Perez-Pariente et al. reported that the porosity in the system  $\text{SiO}_2\text{-CaO-P}_2\text{O}_5\text{-ZnO}$  increased in function of the CaO content [63]. The observed porosity in the interior of the piece owing to the  $\text{Ca}(\text{NO}_3)_2$  decomposition would explain this fact. During decomposition, the high  $\text{Ca}(\text{NO}_3)_2$  content in the dried gel leads to the formation of meso- and macro-porosity higher than 60% in volume. This porosity, together with the high  $\text{Ca}^{2+}$  content, leads to two fundamental effects in the bioactivity process: (a) massive release of  $\text{Ca}^{2+}$  from the glass to the media in a short time, leading to the saturation of the media; and (b) formation of additional porosity during this release, reaching values of 70% after 1.5 h of soaking in SBF [64]. This porosity makes  $\text{Ca}^{2+}$  diffusion from the glass to the SBF easier. It was also observed that the porosity decreased when increasing the  $\text{SiO}_2$  content of the glasses. Our results are in agreement with previous report by P. Saravanapavan and Hench. [65].

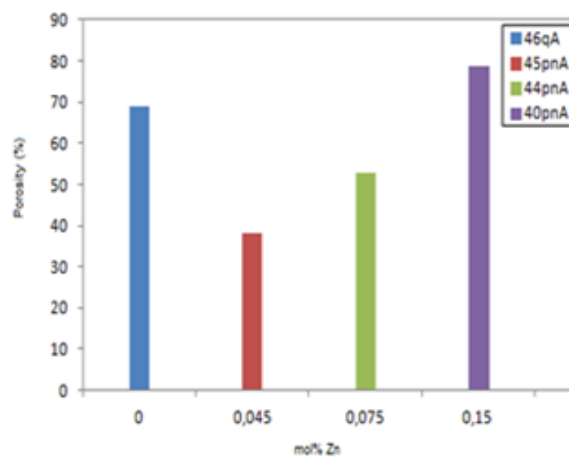


**Figure 8:** Porosity vs. ZnO concentrations of the bioactive glasses 40pnA, 44pnA, 45pnA and 46qA.

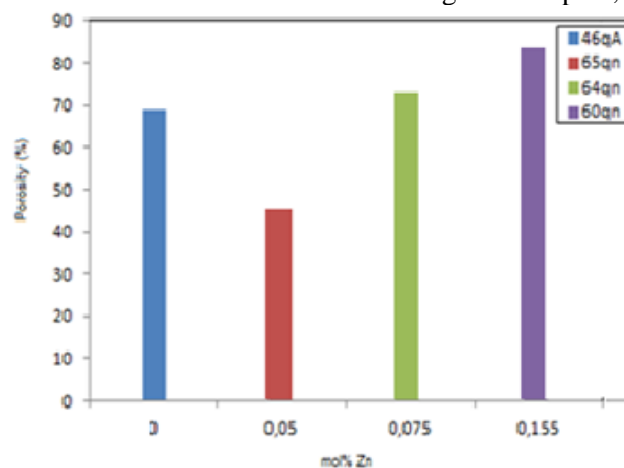


**Figure 9:** Porosity vs. [ZnO] of the bioactive glasses 46qA, 60qn, 64qn and 65qn.

### 3.6. Water and SBF contact angle measurements

Contact angle measurements were recorded to determine the tendency of the bioactive glass surface to absorb water (hydrophilicity) in relation to Zn incorporation in the glass precursors, hence evaluating the bioactive glass surface chemistry. The surface properties will greatly influence the performance of a biomaterial in a biological environment [66]. In fact, the hydrophilicity of material is an important factor for cell adhesion and growth, and improved surface hydrophilicity of materials will improve the interactions between the composites and cells for eliciting controlled cellular adhesion and maintaining differentiated phenotypic expression [67]. Different theories have been proposed to define the hydrophilicity level of a surface. According to Vogler [68], the hydrophilic/hydrophobic character of a material surface can be defined from its contact angle values, taking as reference the "Berg limit" ( $\theta = 65^\circ$ ). Above  $65^\circ$  the surfaces are considered hydrophobic, while they are

hydrophilic below  $65^\circ$ . This criterion is applicable to ideally nonrough surfaces. According to Mittal [69], the wettability of the surface increases with the decrease in contact angle. The water contact angles of the studied bioglasses are presented in Figure 10. For both fluids utilized (distilled water and SBF), the materials presented lowest contact angle values. In this study, contact angles from seven glass samples were measured (Figure 10). The results show that the most hydrophilic surfaces present the lowest contact angle values. 46qA and 40pnA were the most hydrophilic material with water and simulated body fluid respectively. Notice that lower contact angles are associated with both higher roughness and adhesion-ability. It was also shown that hydrophilicity increased with an increase in Zn concentration in the glass series. This confirms the porosity results. Contact angle measurements showed distinct differences between the glass substrates, revealing a stronger dependence on the surface chemical composition. With a contact angle of  $22.1^\circ$ , 46qA is significantly much more hydrophilic than the six other glasses. This might be explained by the fact 46qA presents a higher percentage of  $\text{Na}_2\text{O}$ , and thus releases a great number of  $\text{Na}^+$  ions in the medium, which leads to a very hydrophilic surface [70, 71]. The contact angle values measured with water and with simulated body fluid in the surface of 46qA, 65qn, 64qn and 60qn, remained almost unchanged. In contrast, the contact angle values obtained for 45pnA, for 44pnA and for 40pnA with distilled water, was significantly higher than the angle obtained with simulated body fluid. Even though the simulated body fluid is an aqueous solution supplemented with a variety of components. These results suggest that the complex mixture of components underwent different adsorption mechanisms on the different materials surfaces. Depending on the material affinity, the type, amount and conformation of the adsorbed components will change the surface wettability. According to some authors, contact angle values are one of the best wettability properties to predict the material-cell interactions at the initial stages of contact [72]. Some studies support that hydrophobicity favors the adsorption of adhesive proteins namely fibronectin and fibrinogen, while some authors confirm that a moderate hydrophilicity ( $20\text{-}40^\circ$  water contact angle) leads to maximal adhesion [73]. Our samples present a clear hydrophilic nature; they seem to be in agreement with the above second statement.

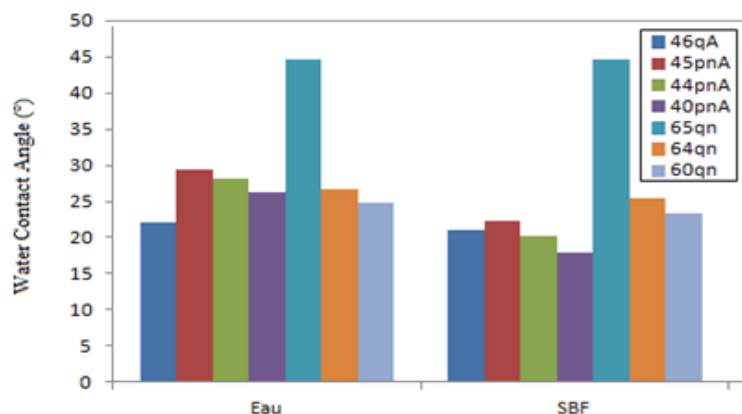
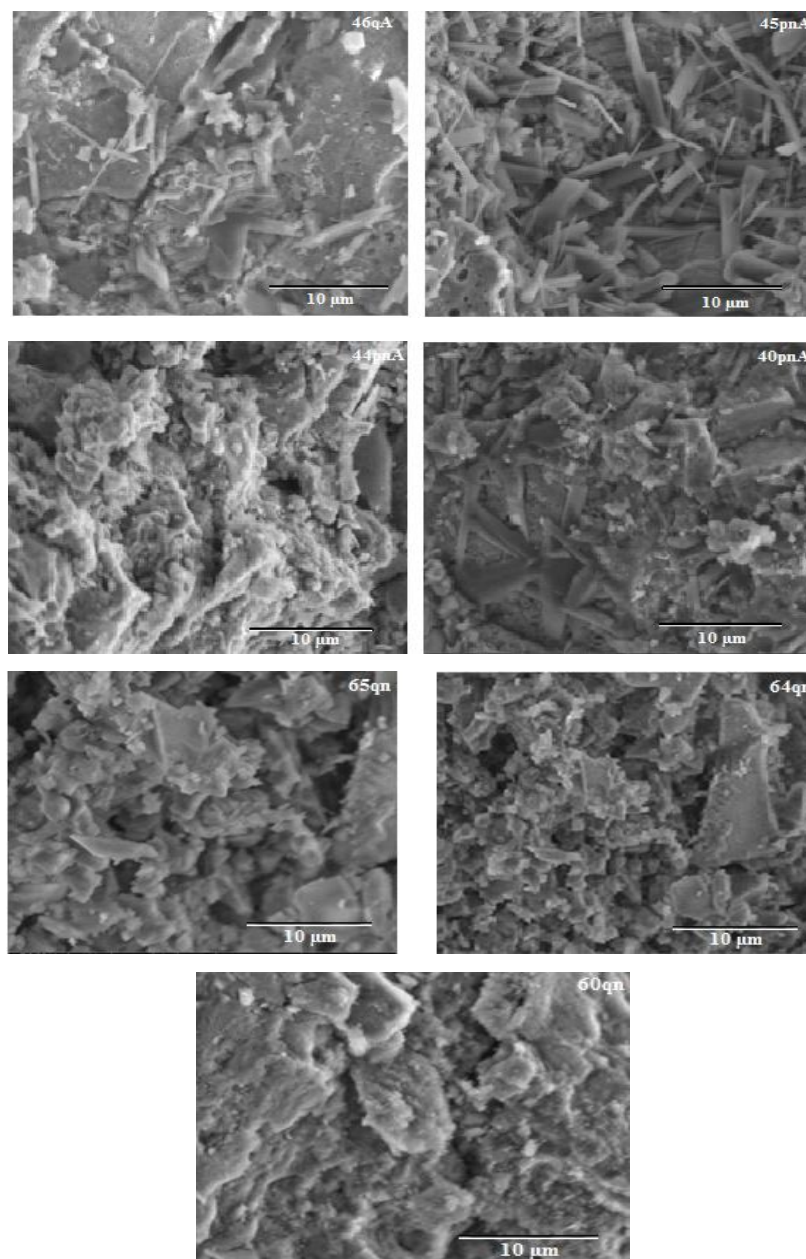


Figure 10: Contact angle measurements for the different fluids for the seven glasses.

### 3.7. Morphology

Figure 11 shows micrographs obtained from the prepared glass samples before soaking in SBF. The glasses are composed of irregular particles, corresponding to glasses obtained by the sol-gel method. The morphology of the glasses are clearly observed, their sizes and their reliefs are different according to the doping element content (ZnO) and to substituted oxide. We were able to study the evolution of porosity as a function of addition of ZnO in the base bioactive glass (46qA). Most of pores of pure and ZnO doped bioactive glass samples were still open due to the optimized characteristics of gel solution and proper removal of the excess gel. Indeed, 46qA, 45pnA, 44pnA and 40pnA have almost the same morphology and the same relief but their size of crystals is different and their particles are more heterogeneous. The micrographs show that the formed crystalline surface has polycrystalline fine texture in comparison with the surface formed on the base bioglass samples (46qA). These micrographs confirm the XRD results showing the presence of two main crystalline phases ( $\text{Na}_2\text{Ca}_2\text{Si}_3\text{O}_9$ ,  $\text{Na}_2\text{CaSi}_3\text{O}_8$ ) for pure glass (46qA) and formation of a new crystalline phase ( $\text{Na}_6\text{Ca}_3\text{Si}_6\text{O}_{18}$ ) for ZnO doped glasses (45pnA), (44pnA) and (40pnA). Whereas Na free and ZnO doped glasses (65qn), (64qn) and (60qn) are homogeneous. This confirms the XRD results showing the amorphous nature of the samples. It was also observed that the porosity of prepared glass samples increased with an increase in ZnO content. Porosity measurements confirmed the obtained results.



**Figure 11:** ESEM images of the bioglasses 46qA, 45pnA, 44pnA and 40pnA 65qn, 64qn and 60qn prepared by the sol-gel method.

## Conclusion

The bioglass powders in  $\text{SiO}_2\text{-CaO-Na}_2\text{O-P}_2\text{O}_5$ ,  $\text{SiO}_2\text{-CaO-P}_2\text{O}_5\text{-ZnO}$  and  $\text{SiO}_2\text{-CaO-Na}_2\text{O-P}_2\text{O}_5\text{-ZnO}$  systems were obtained by a sol-gel method. The sintering temperature of 973K is optimal to provide a reasonable crystallinity for bioactive glass containing  $\text{Na}_2\text{O}$ , while maintaining good bioactivity and high resorbability in physiological fluids. The X-ray diffraction patterns of the bioactive glass show the presence of two main crystalline phases of sodium calcium silicate ( $\text{Na}_2\text{CaSi}_3\text{O}_8$ ,  $\text{Na}_2\text{CaSi}_3\text{O}_9$ ). The effect of introduction of ZnO in  $\text{SiO}_2\text{-CaO-Na}_2\text{O-P}_2\text{O}_5$  system leads to the formation of a new crystalline phase ( $\text{Na}_6\text{Ca}_3\text{Si}_6\text{O}_{18}$ ). The addition of ZnO to glass composition induced significant modifications of the chemical durability and bioactivity. The physicochemical results show the formation of a hydroxyapatite for pure and doped bioactive glasses after soaking in SBF solution. The apatite formation is mainly dependent on amount of ZnO incorporation which appears a good durability in SBF solution. The IR spectra of all the ZnO substituted bioactive glasses in comparison with the base bioactive glasses reveal minor or limited variation of the positions and intensities of the transmittance peaks. The spectra revealed that the intensity of peak decreased with increasing ZnO content. They also showed that after soaking in SBF, the ratio of HCA decreases with ZnO content. The porosity and

hydrophilicity increase also with the ZnO content, in agreement with the contact angle measurements. The pH of the solution with substitution of different oxides after immersed in SBF decreases with increasing of ZnO content. This is probably due to the release of Zn ions into the SBF solution. The slow release of zinc incorporated into the glass is known to promote bone formation around the implant and accelerates the patient's recovery. The studied samples presented a clear hydrophilic nature, all with lower water angles values.

**Acknowledgements**-The authors would like to acknowledge the support and technical assistance of Interface Regional University Center (University Sidi Mohammed Ben Abdellah, Fez), and National Center for Scientific and Technical Research (CNRST-Rabat).

## References

1. Hench L. L., Splinter R. J., Allen W. C., Greenlee T. K., *J. Biomed. Mater. Res.* 5 (1971) 117.
2. Shirliff V. J., Hench L. L., *J. Mater. Sci.* 38 (2003) 4697.
3. Alcaide M., Portoles P., Lopez-Noriega A., Acros D., Vallet-Regi M., Portoles M. T., *Acta Biomater.* 6 (2010) 892.
4. Goudouri O. M., Kontonasaki E., Theocharidou A., Papadopoulou L., Kantiranis N., Chatzistavrou X., Koidis P., Paraskevopoulos K. M., *Mater. Chem. Phys.* 125 (2011) 309.
5. Elshahat A., Shermak M. A., Inoue N., Chao E. Y., Manson P., *J. Craniofac. Surg.* 15 (2004) 483.
6. Fathi M. H., Doostmohammadi A., *J. Mater. Process. Technol.* 209 (2009) 1385.
7. Kokubo T., Kushitani H., Sakka S., Kitsugi T., Yamamuro T., *J. Biomed. Mater. Res.* 24 (1990) 721.
8. Kokubo T., Takamada H., *Biomaterials.* 27 (2006) 2907.
9. Lusvardi G., Zaffe D., Menabue L., Bertoldi C., Malavasi G., U. Consolo, *Acta Biomater.* 5 (2009) 419.
10. Hench L. L., *J. Am. Ceram. Soc.* 74 (1991) 1487.
11. Gerhardt L. C., Boccaccini A. R., *Materials.* 3 (2010) 3867.
12. Peitl O., Zanotto E.D., Hench L. L., *J. Non-Cryst. Solids.* 292 (2001) 115.
13. Siqueira R. L., Peitl O., Zanotto E. D., *Mater. Sci. Eng. C.* 31 (2011) 983.
14. Hench L. L., *J. Am. Ceram. Soc.* 81 (1998) 1705.
15. Chen Q. Z., Boccaccini A. R., *Adv. Eng. Mater.* 8 (2006) 285.
16. Franks K., Abrahams I., Georgious G., Knowles J. C., *Biomaterials.* 22 (2001) 497.
17. Brinker C. J., Scherer G. W., Academic Press, New York. (1990).
18. Balamurugan A., Balossier G., Kannan S., Michel J., Rebelo A. H. S., Ferreira J. M. F., *Acta Biomater.* 3 (2007) 255.
19. Li R., Clark A. E., Hench L. L., *J. Appl. Biomater.* 2 (1991) 231.
20. Zhang K., Washburn N. R., Simon Jr. C. G., *Biomaterials.* 26 (2005) 4532.
21. Olmo N., Martin A. I., Salinas A. J., Turnay J., Vallet-Regi M., Lizarbe M. A., *Biomaterials.* 24 (2003) 3383.
22. Oki A., Parveen B., Hossain S., Adeniji S., Donahue H., *J. Biomed. Mater. Res. A* 69 (2004) 216.
23. Aito ., Otsuka M., Kawamura H., Ikeuchi M., Ohgushi H., Sogo Y., et al., *Curr. Appl. Phys.* 5 (2005) 402.
24. Legeros R. Z., *US Patent.* September 2 (2008) 7- 419.
25. Ito A., Kawamura H., Otsuka M., Ikeuchi M., Ohgushi H., Ishikawa K., Onuma K., Kanzaki N., Sogo Y., Ichinose N., *Mater Sci. Eng. C.* 22 (2002) 21.
26. Courtheoux L., Lao J., Nedelec J-M., Jallot E., *J. Phys. Chem. C.* 112 (2008) 13663.
27. Whitney E. N., Rolfes S. R., Wadsworth Publishing, Belmont (2010).
28. Yamaguchi M., *J. Trace Elem. Exp. Med.* 11 (1998) 119.
29. Lang C., Murgia C., Leong M., Tan L-W., Perozzi G., Knight D., Ruffin R., Zalewski P., *Am. J. Physiol. Lung Cell Mol. Physiol.* 292 (2007) L577.
30. Cousins R. J., *Proc. Nutr. Soc.* 57 (1998) 307.
31. Yamaguchi M., Matsui T., *Peptides.* 17 (1996) 1207.
32. Ovesen J., Moller-Madsen B., Thomsen J. S., Danscher G., Mosekilde L., *Bone.* 29 (2001) 565.
33. D. Boyd, H. Li, D.A. Tanner, M.R. Towler, J.G. Wall, *J. Mater. Sci. Mater. Med.* 17 (2006) 489.
34. T. Kokubo, A/W glass-ceramic: processing and properties. In: L.L. Hench, J. Wilson, editors, Singapore: World Scientific. (1993) 75.
35. Kwok D.Y., Lam C.N.C., Li A., Leung A., Wu R., Mok E., Neumann A.W., *Colloids Surf. A* 142 (1998) 219

36. El-Kady A. M., Ali A. F., *Ceram. Int.* 38 (2012) 1195.
37. Du R. L., Chang J., Ni S. Y., Zhai W. Y., Wang J. Y., *J. Biomater. Appl.* (2006) 341.
38. ElBatal H. A., Azooz M. A., Khalil E. M. A., Soltan Monem A., Hamdy Y. M., *Mater. Chem. Phys.* 80 (2003) 599.
39. Peitl O., Zanotto E. D., Latorre G. P., Hench L. L., "Bioactive Ceramics and Method of Preparing Ceramics", US Patent No. 041079, 1997.
40. Leonor I.B., Baran E.T., Kawashita M., Reis R.L., Kokubo T., Nakamura T., *Acta Biomater.* 4 (2008) 1349.
41. Ashok M., Sundaram N. M., Kalkura S. N., *J. Mater. Lett.* 57 (2003) 2066.
42. Shalini A., Alexis R., Shirin K., Vinay R., Pooja G., Anamika B., *Endodontology.* 27 (2015) 24.
43. Karlsson K. H., Fröberg K., Ringbom T., *J. Non-Cryst Solids.* 112 (1989) 69.
44. Filqueiras M. R., La Torr G., Hench L. L., *J. Biomed. Mater. Res.* 27 (1993) 445.
45. Serra J., Gonzalez P., Liste S., Chiussi S., Leon B., Perez-Amor M., Ylanen H. O., Hupa M., *J. Mater. Sci. Mater. Med.* 13 (2002) 1221.
46. ElBatal H.A., Azooz M.A., Khalil E.M.A., Soltan Monem A., Hamdy Y.M., *Mater. Chem. Phys.* 80 (2003) 599.
47. Stanciu G.A., Sandulescu I., Savu B., Stanciu S. G., Paraskevopoulos K. M., Chatzistavrou X., Kontonasaki E., Koidis P., *J. Biomed. & Pharm. Eng.* 1 (2007) 34.
48. Dietrich E., Oudadesse H., Lucas Girot A., Mami M., *J. Biomed. Mater Res.* 88A (2008) 1087.
49. ElBatal H., ElKhesheh A., *Mater. Chem. Phys.* 110 (2008) 352.
50. Mosbahi S., Oudadesse H., Elfeki H., Trigui M., Wers E., Rebai T., Elfeki A., Keskes H., *Inter.J. Eng. Innov. Tech.* 3 (2014) 197.
51. Verne E., Bretcanu O., Balagna C., Bianchi C.L., Cannas M., Gatti S., Brovarone C. V., *J. Mater. Sci-Mater. M.* 20 (2009) 75.
52. Zhong J.P., La Torre G.P., et al., *Bioceramics.* 7 (1994) 61.
53. Kokubo T., Novel bioactive materials. *An. Quim. Int. Ad.* 93 (1997) S49.
54. Jones J.R. Review of bioactive glass: From Hench to hybrids. *Acta Biomater.* 9 (2013) 4457.
55. Abbasi Z., Bahrololoom M., Shariat M., Bagheri R., *J. Dent. Biomater.* 2(1) (2015) 1.
56. Madan N., Sharma V., *J. Acad. Adv. Dent. Res.* 2 (2011) 45.
57. Narayana S.S., Deepa V.K., Ahamed S., *J. Indian. Soc. Pedod. Prev. Dent.* 32 (2014) 19.
58. Jurczyk M.U., Jurczyk K., Miklaszewski A., Jurczyk M., *Mater. Design.* 32 (2011) 4882.
59. Hulbert S. F., Young F. A., Mathews R. S., Klawiter J. J., Talbert C. D., Stelling F. H., *J. Biomed. Mater Res.* 4 (1970) 433.
60. Goldstein S. A., *J. Biomech.* 20 (1987) 1055.
61. Mosbahi S., Trigui M., Jebahi S., Farhat L., Oudadesse H., Reabai T., Daoued J., Kekes H., *Eur. Cells. Mater.* 28(5) (2014) 38.
62. Jones J. R., Hench L. L., *J. Biomed. Mater. Res. B.* 68 (2004) 36.
63. Perez-Pariente J., Balas F., Roman J., Salinas J., Vallet-Regi M., *J. Biomed. Mater Res.* 61 (2002) 524.
64. Rahaman M. N., Day D. E., Bal B. S., Fu Q., Jung S. B., Bonewald L. F., Tomsia A. P., *Acta Biomater.* 7(6) (2011) 2355.
65. Saravanapavan P., Hench L. L., *J. Biomed. Mater. Res.* 54 (2001) 608.
66. Wu C., Ramaswamy Y., Boughton P., Zreiqat H., *Acta Biomater.* 4 (2008) 343.
67. Yusuke A., Hiroo I., *Biomaterials.* 28 (2007) 3074.
68. Vogler E. A., *Adv. Colloid Interface Sci.* 74 (1998) 69.
69. Mittal K. L., Contact Angle, Wettability and Adhesion, 4th ed.; CRC: New York, NY, USA, 2006.
70. De Rosa R. L., Schader P. A., Shelby J. E., *J. Non-Cryst. Solids.* 331 (2003) 32.
71. Bouhazma S., Chajri S., Barkai H., Elabed S., Ibsouda Koraichi S., El Bali B., Lachkar M., *Mor. J. Chem.* 3(1) (2015) 19-27.
72. Lampin M., Warocquier-Clerout R., Legris C., Degrange M., Sigot-Luizard M. F., *J. Biomed. Mater. Res.* 36 (1997) 99.
73. Khang G., Jeon J. H., Lee L. W., Cho S. C., Lee H. B., *Biomed. Mater Engl.* 7 (1997) 357.